ELSEVIER

Nuclear Instruments and Methods in Physics Research B 145 (1998) 434–448

NIM B
Beam Interactions with Materials & Atoms

A method for forward energy-dispersive X-ray fluorescence analysis of thin and intermediate samples

Roberto Cesareo [a,*], Giovanni E. Gigante [b], Albert L. Hanson [c]

[a] *Istituto di Matematica e Fisica, Università di Sassari, Via Vienna 2, I-07100 Sassari, Italy*
[b] *Dipartimento di Fisica, Università di Roma "La Sapienza", Rome, Italy*
[c] *Brookhaven National Laboratory, Upton, LI, New York, USA*

Received 5 May 1997; received in revised form 2 July 1998

Abstract

The usefulness of forward geometry in Energy Dispersive X-Ray Fluorescence (EDXRF) analysis has been investigated both experimentally and theoretically. This work relates to milli- and micro-beams, which limits this work to tightly collimated incident X-ray beams (<1 mm). The use of forward geometry also limits the targets to be of thin and intermediate thickness. The advantages and the peculiarities of using a forward geometry for XRF are discussed. Forward X-Ray Fluorescence (FXRF) has features including: (a) high geometrical efficiencies when using tightly collimated primary beams; (b) a minimisation in the uncertainty in the interaction volume; (c) a sample thickness at which the production of characteristic X rays is maximised; and (d) a filtering action by intermediate thickness samples resulting in an enhancement of the sensitivity for higher atomic number elements with respect to lower atomic number elements. For thin and intermediate thickness samples simultaneous forward and backward geometry XRF can be used to correct for self-absorption effect.

1. Introduction

In X-Ray Fluorescence (XRF) analyses two measures of performance are commonly quoted, the first being the Minimum Detectable Limit (MDL) and the second being the ratio of the fluorescence intensity (the portion of the spectra of the interest) to the spectral background (P/B ratio) [1]. The main difference between these two performance measures is that the MDL is proportional to the square root of the background divided by the fluorescence intensity and the P/B ratio is a straight ratio of the fluorescence intensity divided by the background. While the MDL tells us how well the technique can ultimately analyse elements, it is more complicated than the simple P/B ratio since time of data acquisition is now involved. This means that, ignoring statistical effects, the MDL continually improves with acquisition time, while the P/B ratio does not.

Improvements in both the MDL and P/B ratio can be achieved by increasing the total number of fluorescence X rays, which usually can be achieved

* Corresponding author. Tel.: 079-229-481; fax: 079-229-482.

0168-583X/98/$ – see front matter
PII: S0168-583X(98)00418-2

only with an increase in total number of incident X rays. Once a detector system has reached it's throughput limit, increasing the detected fluorescence intensity is no longer possible. Therefore further improvements in the MDL and P/B ratio can be achieved only by reducing the background, most of which results from the scattering of the incident radiation.

Reducing the background from scattered radiation can be achieved by polarising or monochromatising the incident radiation, or both. By polarising the incident radiation the scattering cross section can be minimised. By monochromatising the radiation, the energy band that the X rays are scattered into is reduced. When the excitation beam is "white", or the bremsstrahlung radiation straight from an X-ray tube, the scattered X-ray spectra is continuous, just shifted to lower energies from the incident spectra. However, by monochromatising the incident X-ray beam, the scattered radiation is a small band shifted in energy by the Compton scattering relation [2], the atomic Compton scattering being the dominant process for most XRF systems. This shift can become troublesome for the higher excitation energies (>15 keV). Even though this energy band is relatively narrow it is broadened by the "Compton profile" and is usually the broadest peak in the spectra [3]. Implementation of these techniques has led to an improvement in the ratio of the fluorescence peak intensity (the portion of the spectra of interest) to the background from scattered radiation [4].

Creating a source of monochromatic X rays from an X-ray tube has usually been achieved with X-ray diffraction. However, diffraction is a low efficiency process, so the resulting intensity is usually low [5]. Two other methods of creating quasi-monochromatic X-ray beams employs either a secondary target or a critical filter [6]. Both of these methods were used for this paper. The secondary target technique is illustrated in Fig. 1 and uses an X-ray tube in the reflection mode to excite characteristic K_α and K_β X rays of the secondary target. These characteristic X rays from the secondary target are used for the excitation. The critical filter technique is demonstrated in Fig. 2. For this technique the X-ray beam passes through a filter chosen to absorb X-rays below a particular energy [7].

One important aspect of XRF that should always be considered is the geometrical efficiency especially in the construction of milli- and microprobes. The geometrical efficiency can be maximised by using small sample–detector (r_D) and sample–source (r_S) distances though it is easier to reduce r_D in the forward geometry (denoted as FXRF).

The MDL of an XRF system is typically in the range of nanograms to micrograms. The actual MDL attained depends on characteristics of: the XRF source, which determines the energy distri-

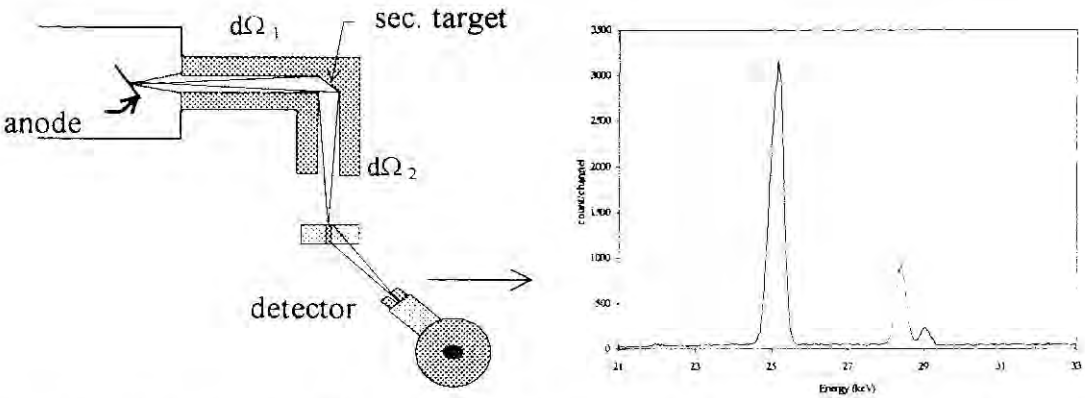

Fig. 1. Geometry for the forward XRF technique when using a secondary target as the source of monochromatised radiation. The X-ray spectra from the secondary target is shown.

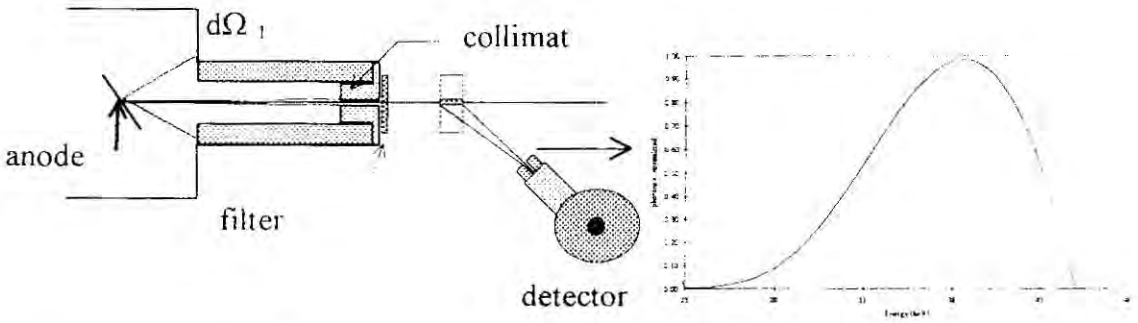

Fig. 2. Geometry for the forward XRF technique when using a filter to produce a beam of quasi-monochromatic radiation. The X-ray spectra of the filtered radiation is shown.

bution of the incident X rays; the detector, which determines the energy resolution of the fluorescence X rays peak along with the detection efficiency; the target, since the thickness and matrix determine the transmission and the scattered radiation; and the measurement time. Typical analysis times are of the order of 10^3 s. The MDL decreases (improves) with the square root of the irradiation time and the square root of the exciting radiation intensity. Even though the MDL nominally improves with the exciting radiation intensity, this improvement is not infinite since there are technical limits on the throughput that the detector and associated electronics, can process; typically no more than 10^3–10^4 counts/s. The ultimate MDL is also limited by the geometrical efficiency. A typical X-ray source provides 10^9 photons/cm^2/s for fluorescing the elements of interest. With this intensity of incident radiation, a sample containing 1 μg of a trace element in the interaction volume, with $25 \leqslant Z \leqslant 92$, will give rise to tens to hundreds of fluoresced photons/s.

For this paper, the technique of performing XRF in a microanalysis mode with forward geometry FXRF has been investigated both theoretically and experimentally. Because of forward geometry, "thin" and "intermediate" thickness samples are required. In this sense the term "thin" means the attenuation of radiation through the sample is not significant. The term "intermediate" implies some attention occurs. It will be shown that with FXRF one can enhance the analysis of selected elements, when samples of varying thickness are available. This fact can be utilised when higher Z trace elements are being analysed in lower Z matrices. This contrast is not atypical in the analysis of biological samples and many geological samples. The forward geometry has one advantage over the typical normal geometry in that the uncertainty in the volume being sampled is smaller, because the target is no longer placed at a 45° angle.

2. Theoretical background

The fluorescent flux from an element a produced at a depth x (g/cm^2) is given by (see Fig. 3a and Table 1):

$$dI_a = A w_a \, e^{-\mu_0(\underline{x}-x)} \, e^{-\mu_a \underline{x}} \, dx \text{ in the forward direction,} \quad (1a)$$

$$dI_a = A w_a \, e^{-\mu_0 x} \, e^{-\mu_a \underline{x}} \, dx \text{ in the backward direction,} \quad (1b)$$

where $\underline{x}$ represents the mass per unit area of the sample. For these equations, it has been assumed that the incident and fluoresced X rays enter and exit the target normal to the target's surface (Fig. 3a). In both cases $\varphi = \pi/2$. For the case of FXRF $\psi = -\pi/2$ and $\theta = 180°$ (Fig. 3b). In real situations, these assumed values are limits, but invoking these assumptions greatly simplify the mathematics without considerable accuracy. Note that for this paper we are emphasising "thin" and "intermediate" thickness samples, so the forward scattering and its associated build-up factor are not significant.

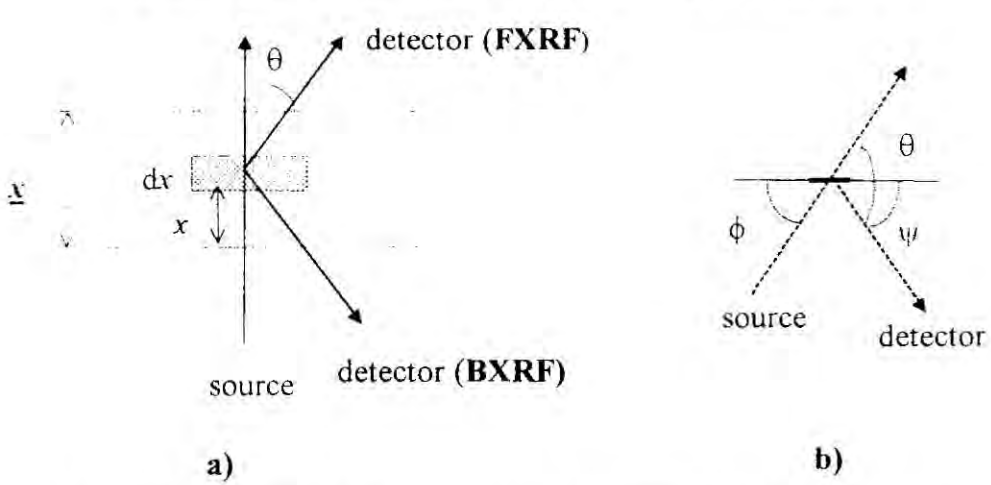

Fig. 3. Schematic drawing of the possible geometrical arrangements in the XRF techniques.

For Eqs. (1a) and (1b), the factor A is the production rate per unit weight fraction and mass per unit area (g/cm^2) for the characteristic X rays from element a:

$$A = I_0 k \varepsilon(E_a) \mu_{ph,a}(E_0) \omega_{a,s} F_{a,s} p_l. \quad (2)$$

The symbols of Eq. (2) are listed in Table 1. Note that the values of μ's refer to the whole specimen and can be determined as a linear summation over all of the target's elements:

$$\mu_0 = \sum_i w_i \mu_{0,i}. \quad (3)$$

The intensity of the fluoresced X rays into the backward direction (BXRF) is obtained by integrating Eq. (1b) over x:

$$I_a = A w_a \frac{1 - e^{-(\mu_a + \mu_0)\underline{x}}}{\mu_a + \mu_0}. \quad (4)$$

Fig. 4 shows log–log plots of Eq. (4) for the backward geometry fluorescence of K_α X rays of sulphur, calcium, iron, selenium and strontium in a water matrix for a primary excitation beam of 17.5 keV. To simplify the reading of figures, for this and all subsequent figures the primary beam intensity was assumed to be $I_0 = 10^6$ photons/cm^2 s and the weight fraction equal to 1 ppm (μg/g). In this way the product of the two coefficients is equal to one. Also the efficiency factor k, i.e. the product of the geometrical and the physical efficiency, is set equal to one. Each curve can be subdivided into three regions [2]: (1) the first is the "thin" sample region which has an upper bound of

Table 1
List of symbols employed in this paper

I_a (photons/cm^2 s)	Fluorescent photon fluence rate (number of photons per unit area and time) of X rays of element a
I_0 (photons/cm^2 s)	Incident photon fluence rate
k	Efficiency term taking into account for physical and geometrical efficiency
$\varepsilon(E_a)$	Intrinsic detector efficiency at the energy of the line of the element a
$\mu_{ph,a}(E_0)$ (cm^2/g)	Photoelectric mass attenuation coefficient of element a at incident energy E_0
$\omega_{a,s}$	Fluorescent yield of element a for the shell s = K,L, ...
$F_{a,s}$	Fraction of photoelectric interactions occurring in the shell s
p_l	Probability that the fluorescence event belongs to the l = α,β,γ,... line of interest
w_a	Weight fraction of element a
μ_0 and μ_a (cm^2/g)	Total mass attenuation coefficients of the sample for incident and fluorescent energy respectively
μ_s (cm^2/g)	Coherent + Compton scatter mass attenuation coefficient of the sample at incident energy

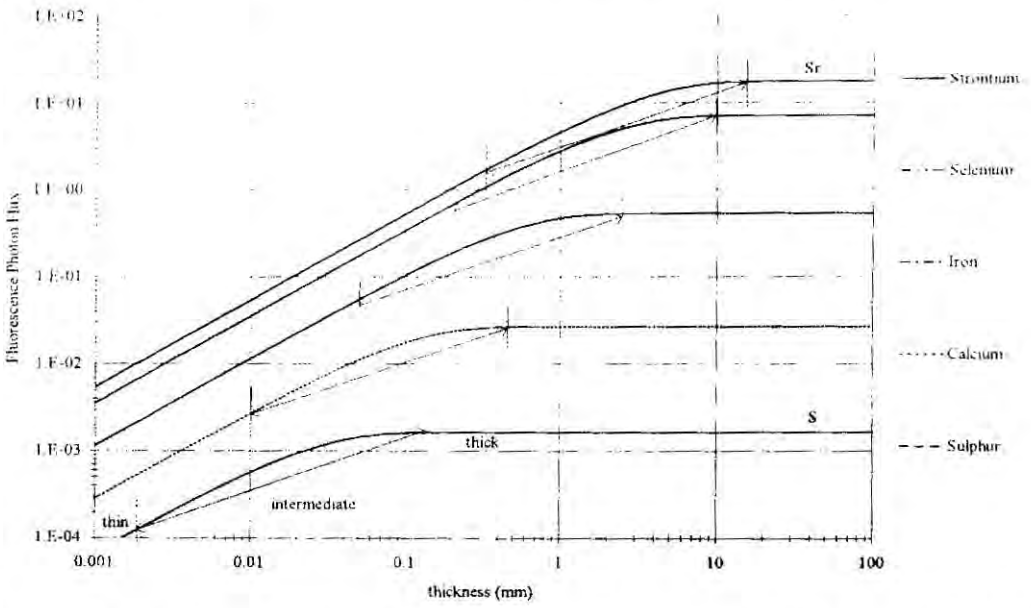

Fig. 4. Plot of the backward geometry fluorescence photon flux photons/cm^2 s for the K_α-lines of some elements dissolved in a water matrix to a concentration of 1 ppm when excited with an incident X-ray energy of 17.5 keV. Thin, intermediate and thick regions are shown.

$((\mu_a + \mu_0)\underline{x}_{thin}) = 0.1$; (2) the second is the "thick" sample region which has a lower bound of $((\mu_a + \mu_0)\underline{x}_{thick}) = 4.6$; and (3) the third is the "intermediate" thickness region which is bounded by the thick and thin regions. For the fluorescence of elements at 1 ppm in a water matrix, Fig. 5 shows the values of $\underline{x}_{thin}$ and $\underline{x}_{thick}$ as a function of element for elements between Ca and Zr. Also shown on this curve is the value of $\underline{x}_{max}$ which is given below in Eq. (6). Any water sample thicker than the upper line is a "thick" sample; any water sample thinner than the lower line is a "thin" sample, and any water sample in between is an "intermediate" sample.

In the backward direction, the thin sample region is characterised by an increase of fluoresced X-ray intensity which is linear with sample thickness. In the intermediate sample region the increase in fluoresced X-ray intensity is non-linear with sample thickness; the increase in fluoresced X-ray intensity having a lower, variable slope. Finally, in the thick sample region, the fluoresced X-ray intensity has saturated so it is independent of the sample thickness. Selected values from Fig. 4 for the elements sulphur, calcium, iron, selenium and strontium are reported in Table 2.

In the forward direction (FXRF) the intensity of the fluoresced X rays is obtained by integrating Eq. (1a) over x

$$I_a = Aw_a e^{-\mu_0 \underline{x}} \int_0^{\underline{x}} e^{-(\mu_a - \mu_0)x}\,dx$$
$$= Aw_a e^{-\mu_0 \underline{x}} \frac{1 - e^{-(\mu_a - \mu_0)\underline{x}}}{(\mu_a - \mu_0)}. \quad (5)$$

Fig. 6 shows log–log plots of Eq. (5) for the fluorescence of the K_α X rays of sulphur, calcium, iron, selenium and strontium in a water matrix at a concentration of 1 ppm. The primary excitation beam was 17.5 keV.

A comparison of Figs. 4 and 6 demonstrates that the fluorescence intensities are similar for thin and intermediate samples in both the forward and backward directions. However, there are substantial differences in the FXRF and BXRF for the thick samples. For the BXRF case the fluorescence intensity from thick samples has saturated because X rays generated "deep" in the samples are totally attenuated by the matrix. For FXRF two effects

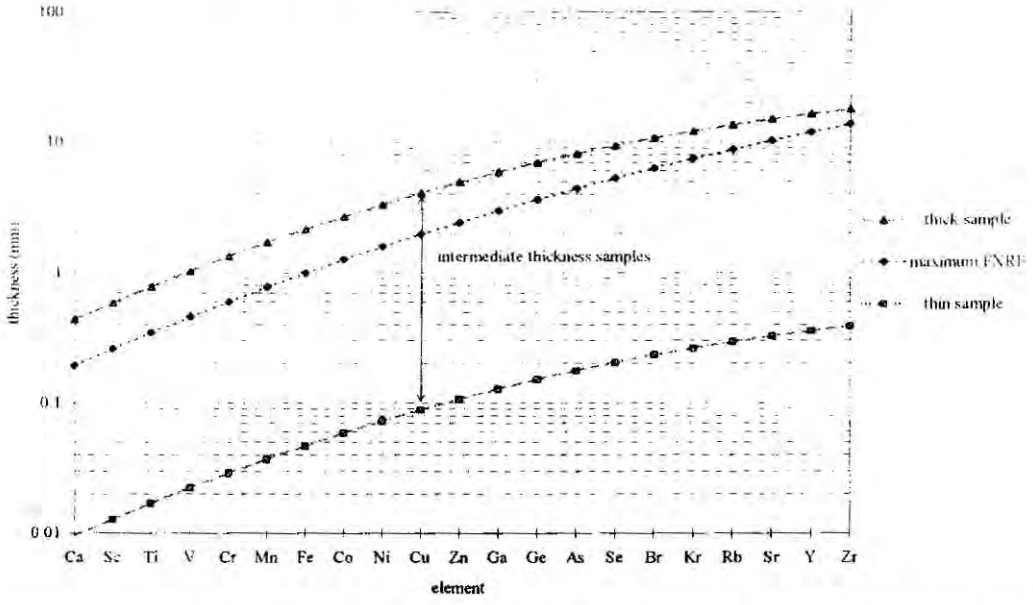

Fig. 5. Thin sample approximation upper limits (lower curve), thick sample approximation lower limits (upper curve) and maxima of FXRF fluxes (middle curve) for elements in the Z interval between Ca and Zr in a water matrix at a concentration of 1 ppm with an incident energy of 17.5 keV.

occur. First the X rays generated near the front surface (the surface not seen by the detector) of the sample are attenuated but the fluorescing beam has also been attenuated. Therefore for FXRF the fluorescence intensity continually decreases exponentially with increasing sample thickness as both the incident beam and the fluoresced X rays are attenuated.

For FXRF, there is a sample thickness for which the fluoresced X-ray intensity is a maximum, which means for FXRF the sample thickness can never be neglected. The sample thickness $\underline{x}_{max}$ at which this maximum occurs can be calculated with the relation:

$$\underline{x}_{max} = \frac{\ln(\mu_a/\mu_0)}{\mu_a - \mu_0}. \tag{6}$$

Fig. 5 (middle curve) demonstrates that the $\underline{x}_{max}$ for the FXRF increases with Z. This fact can be utilised to preferentially enhance the fluorescence of higher Z elements with respect to lower Z elements. This enhancement can be important for certain matrices.

In order to emphasise the similarities and differences between BXRF and FXRF, Fig. 7 shows plots of Eqs. (4) and (5) for the K_α fluorescence of 1 ppm Fe in a water matrix excited with an incident X-ray beam of 17.5 keV. Eqs. (4) and (5) have the same results for both thin and the lower part of the intermediate thickness regions. They start deviating in the higher part of the intermediate thickness region.

It is also instructive to plot the ratio of the BXRF/FXRF intensities:

$$\frac{1 - e^{-(\mu_a+\mu_0)\underline{x}}}{\mu_a + \mu_0} \frac{\mu_a - \mu_0}{1 - e^{-(\mu_a-\mu_0)\underline{x}}} e^{\mu_0 \underline{x}}, \tag{7}$$

Table 2
Forward intensities of S, Ca, Fe, Se and Sr in water matrix, at an incident energy of 17.5 keV

Sample thickness:	10 μm	100 μm	1 mm	1 cm
S	0.00056	0.0016	0.0016	0.0016
Ca	0.00265	0.017	0.026	0.026
Fe	0.011	0.10	0.47	0.53
Se	0.035	0.34	2.75	7.08
Sr	0.053	0.52	4.54	16.48

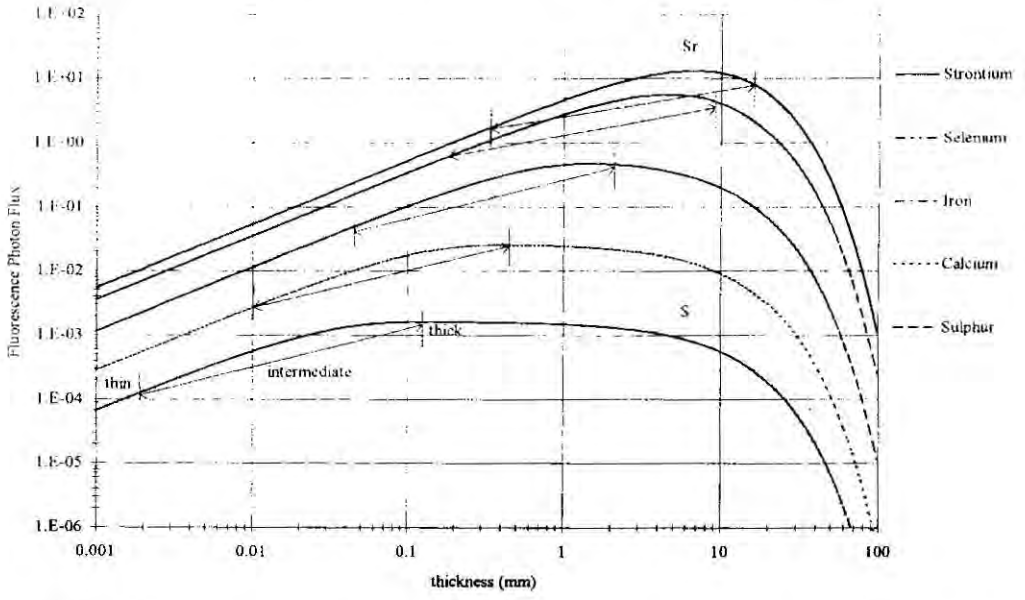

Fig. 6. Plot of the forward geometry fluorescence photon flux photons/cm² s for the K_α-lines of some elements dissolved in a water matrix to a concentration of 1 ppm when excited with an incident X-ray energy of 17.5 keV. The upper limit of thin sample intervals and the lower limit of the thick sample intervals are also shown.

Fig. 8 shows plots of Eq. (7) for the previously described elements in a water matrix. This figure demonstrates that the BXRF is equal to the FXRF for thin and intermediate thickness samples. In the thick sample region the ratio of BXRF/FXRF increases exponentially. This effect can be deduced from Eq. (7) since for thick targets the two negative exponents can be neglected.

Most of the spectral background is the result of X-ray scattering, so this aspect of X ray interactions needs to be considered. At the energies of most XRF, as far as attenuation is concerned, it can be assumed that the Compton scattered X-rays have the same energy as the Rayleigh scattered X rays. In the backward direction the intensity of the scattered X rays can be written as:

$$I_{sc} = I_0 k \varepsilon(E_{sc}) \sum_i \mu_{sc,i} w_i \frac{1 - e^{-2\mu_0 x}}{2\mu_0}. \quad (8)$$

The summation over i is required now since all atoms in the matrix contribute to the scattered X rays, which is in contrast to the fluorescence of characteristic X rays where only the element of interest is considered.

In the forward direction the intensity of scattered X rays is given by

$$I_{sc} = I_0 k \varepsilon(E_{sc}) \sum_i \mu_{sc,i} w_i x e^{-\mu_0 x}. \quad (9)$$

The ratio of the scatter intensities in the backward to forward direction is approximately unity for thin and intermediate thickness samples.

One final aspect of X-ray interactions that need to be considered here is the geometrical efficiency. This efficiency describes the interaction volume which is the intersection of two volumes: the volume subtended by the incident X-ray beam and the volume subtended by the detector solid angle. It is defined as the product of those two solid angles Ω_S, Ω_D

$$\varepsilon_g = \Omega_D \Omega_S = \frac{A^2 \sin(\varphi) \sin(\psi)}{(4\pi)^2 r_D^2 r_S^2}, \quad (10)$$

where the sum $(\varphi + \psi)$ is equal to the scattering angle (θ) (see Fig. 3b). Here A is the beam spot area, r_S is the source–sample distance, and r_D is the detector–sample distance. The most common geometry for XRF has the scattering angle being 90°.

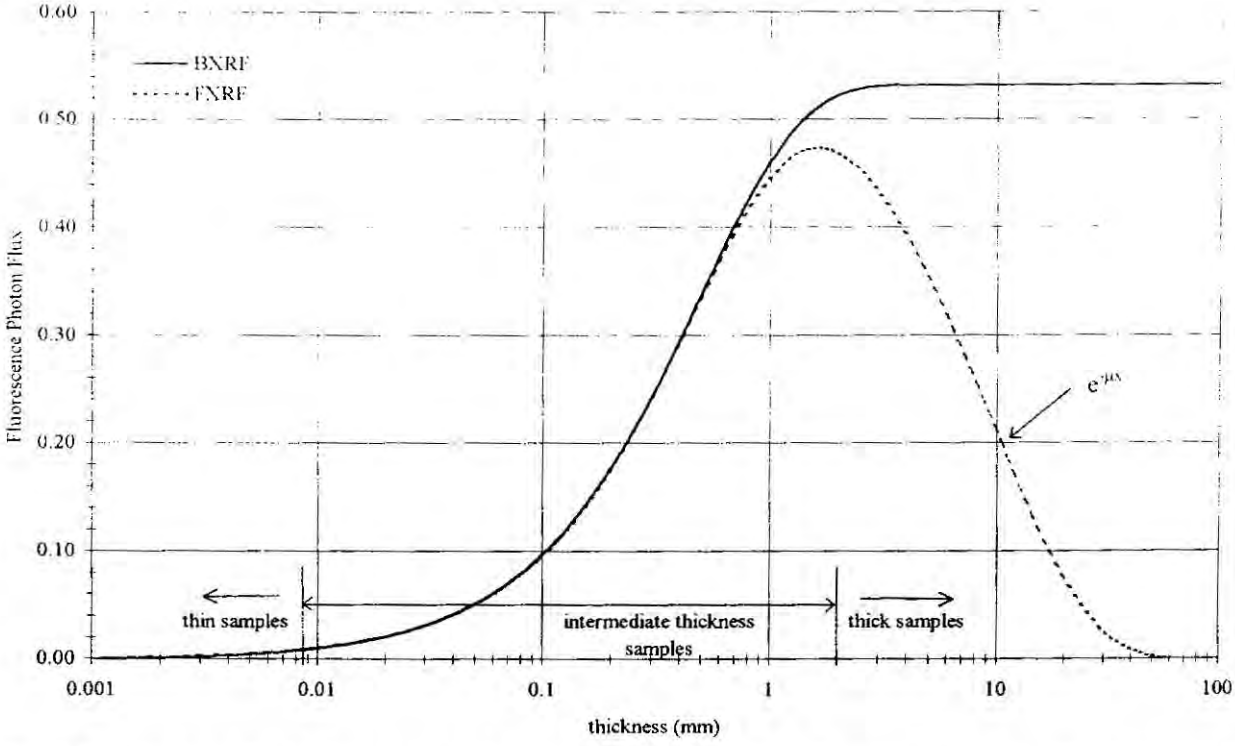

Fig. 7. Plot of the forward and backward geometry fluorescence photon flux for the K_α-lines of iron in a water matrix at 1 ppm excited with an incident X-ray energy of 17.5 keV. The intervals of thin, intermediate and thick samples are shown.

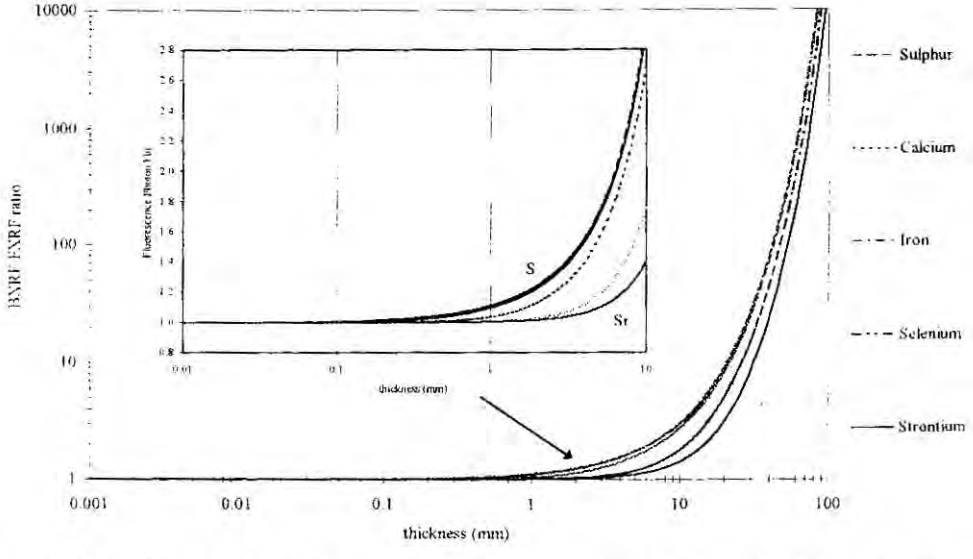

Fig. 8. Plot of the BXRF/FXRF ratio vs. target thickness for the fluorescence of the K_α-lines of S, Ca, Fe, Se, and Sr in a water matrix at a concentration of 1 ppm when excited with 17.5 keV X rays.

For this case it is easy to demonstrate that the geometrical efficiency is maximum when $\phi = \psi = 45°$. However, in order to obtain the best lateral spatial resolution for a given source collimation, we must make $\phi = \pi/2$ (see Fig. 9): in this case Eq. (10) can be simplified:

$$\varepsilon_g = \frac{A^2 \cos(\theta)}{(4\pi)^2 r_D^2 r_S^2}. \tag{11}$$

From Eq. (11), it is possible to deduce that the geometrical efficiencies can be maximised when $\theta = 0$ or π. The uncertainty in the efficiency ($d\varepsilon_g$) is thus minimised when $\theta = 0$ or π. However, referring to Fig. 9, it is evident that $\theta = \pi$ can never be reached because of the presence of the source and that $\theta = 0$ can never be reached because the transmitted and coherently scattered radiation would saturate the detector system.

The geometrical efficiency can be increased by using short values of r_S and/or r_D, especially when using low brilliance X-ray sources such as X-ray tubes. It is easiest to reduce r_D in the forward geometry. Therefore, the forward geometry FXRF results in not only the highest geometrically efficiency but also in the lowest uncertainty in the efficiency. Both of these considerations are important considerations for analyses requiring tight collimation. The overlap of the Ω_s and the Ω_D are shown in Fig. 9. When using tight (circular) collimation and having the beam orthogonal to the surface, the fluorescence volume (defined by Ω_v) approaches a cylinder. By using the forward geometry, the detector then sees a regular cylindrical shape, which has several advantages in tightly collimated systems such as microprobes. Conventional XRF has the detector placed at a right angle to the source with the sample placed at 45°. The result is a sample volume that has an irregular shape which results in the worst case for the lateral resolution. In a microprobe, the beam may exit the target with a significant displacement from the entrance which can cause the actual spatial resolution to be larger than is desired or intended. This can result in substantial edge effects and higher uncertainties in the sampled volumes.

3. Materials and methods

For this work, several samples were fluoresced with different combinations of X-ray tubes and detectors. The experimental set-up consisted of:

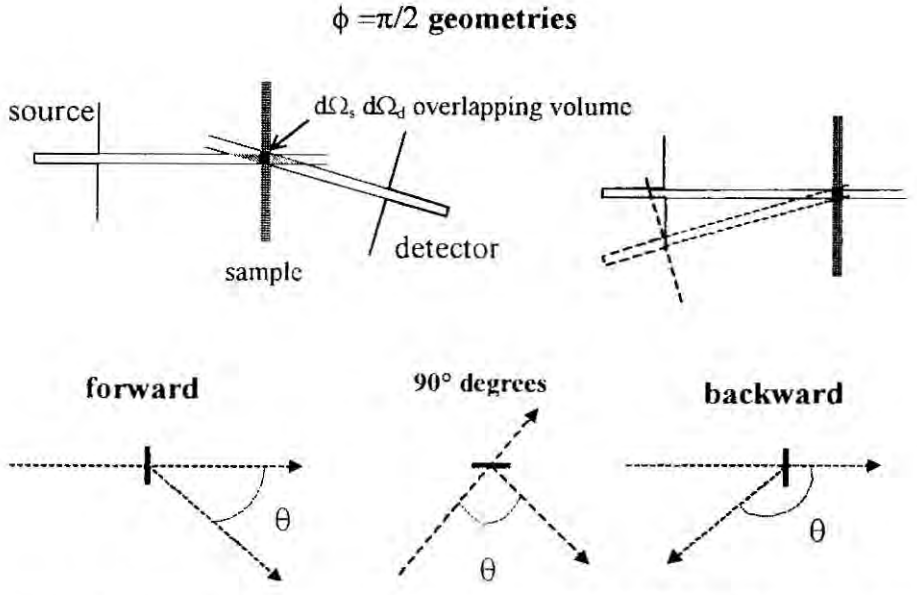

Fig. 9. Schematic drawing illustrating the advantages of using $\phi = \pi/2$ in the forward and backward geometries. In backward geometry the presence of the source hinders the positioning of the detector at very low angles.

- X-ray tubes (Gilardoni, Italy, 20–80 kV, 5 mA, W-anode; EIS, Italy 10–40 kV, 1 mA, W-anode; Oxford, USA, 30 kV, 0.1 mA, W, Pd, Mo anodes) which can be collimated down to 5 μm by using Pt–Ir pinholes.
- 2 detectors: First is an AMPTEK, USA, 300 μm thick Si-PIN detector with an energy resolution of approximately 250 eV at 5.9 keV, with sufficiency detection efficiency in the energy range of 4–30 keV [9]. The second detector is a 3 mm thick HpGe detector with and energy resolution of 160 eV at 5.9 keV. The Si-PIN detector has been studied since it shows promise for portable XRF systems and for BXRF and FXRF because it is compact in size and does not require liquid nitrogen cooling.
- Intermediate thickness samples of various materials, composed of disks 1–2 mm thick epoxy resins containing the elements of interest at concentrations of 1–2%. Samples of marine sediments and multi-minerals characterised as being of intermediate thickness [8].
- Solutions in water with molybdenum mass between 1.9 ng and 245 pg in the scattering volume. These solutions were put in Plexiglass containers of 1×1 cm^2 internal section. The thickness for this is $((\mu_a+\mu_0)x)=1.6$, so these were in the thin/intermediate thickness region.
- A 5 mm thick disk of molybdenum oxide in epoxy resins with molybdenum concentration of 3% in the scattering volume.

4. Results and discussion

Various samples of different thicknesses were examined using the FXRF technique in order to investigate any advantages over conventional XRF. It was demonstrated before that BXRF and FXRF have certain geometrical advantages. From

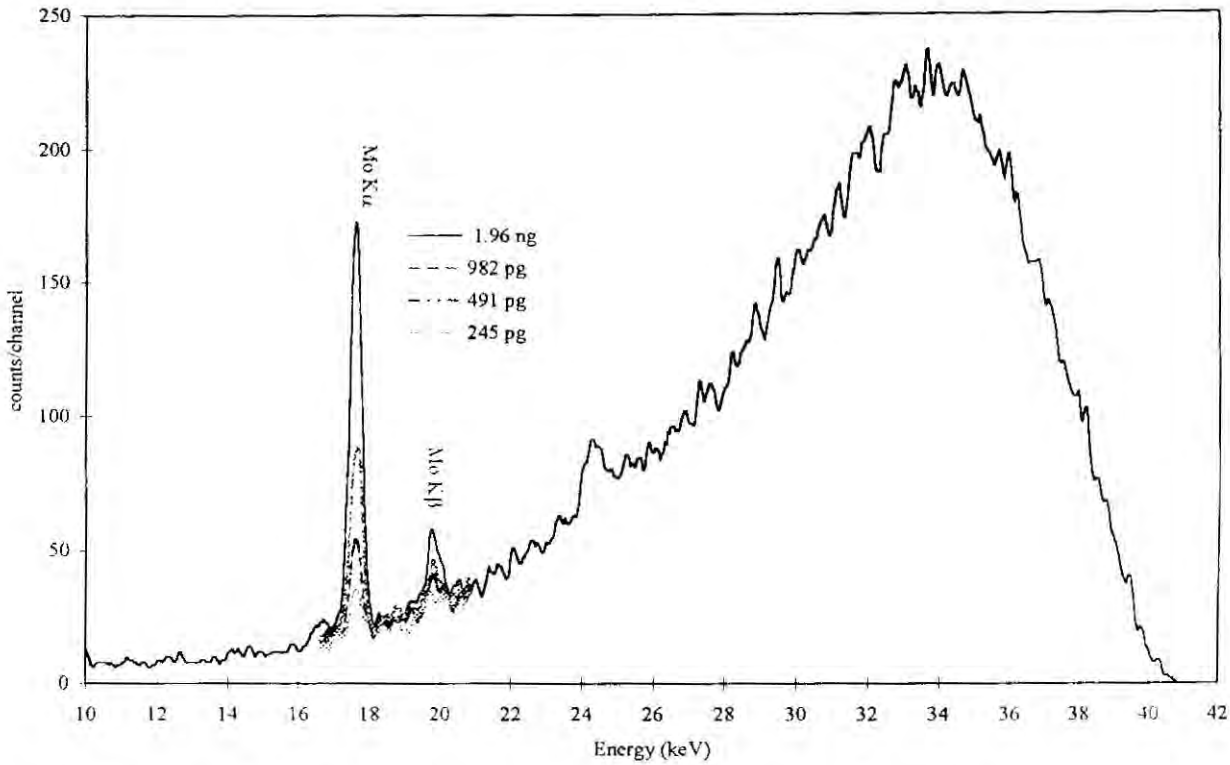

Fig. 10. FXRF-spectra of solutions of molybdenum in water using the geometry of Fig. 2. The spectra were collected with a HpGe-detector counting for 1000 s. A 5 μm diameter collimator was used to define the beam size. An MDL of about 30 pg was obtained.

the theoretical development we see that there is little difference between the BXRF and FXRF in the thin and the lower portion of the intermediate thickness region. However, we will only emphasise measurements using the forward geometry.

In the first set of measurements, the molybdenum samples were studied. These molybdenum samples were irradiated with both bremsstrahlung radiation (42 kV and 5 mA), per Fig. 2, and with X rays from an Sn secondary target, per Fig. 1. In both cases, 5 μm collimators were used to define the incident beam. The HpGe detector was placed at 20° in the forward direction and had a 1 mm collimator on it. Typical X-ray spectra, counting for 1000 s, from of the molybdenum solutions using the filtered radiation are shown in Fig. 10. The calibration curve from the analyses of the Mo solutions is shown in Fig. 11. It appears that the absolute MDL of approximately 35 pg, which is better than the corresponding value for normal incidence XRF. The forward geometry allows for tight collimation while maintaining a good fluorescence counting rate.

One area where milli- and micro-probes are used is in the analysis of physically small mineral grains in larger matrices. Fig. 12 shows the results of FXRF scans across a 1 cm diameter disk of epoxy resin embedded with grains of tin between 20 and 100 μm in size. The source was collimated to 5 μm. While milli- and micro-probes are useful for the analyses of small grains in large matrices, these probes are not well suited for the analyses of inhomogeneous samples, unless it is the non-homogeneity that is of interest.

A third set of samples included multi-mineral pastilles of various thickness. The concentrations of the major elements in the pastille are: P: 9.11%; Cl: 2.7%; K: 2.96%; Ca: 9.93%; Mn: 0.14%; Fe: 1.04%; Cu: 0.15%; and Zn: 1.11%. The following elements are present in trace levels: V: 7.4 ppm; Cr: 18.5 ppm; Ni: 3.7 ppm; Se: 18.5 ppm; Mo: 18.5 ppm; Sn: 7.4 ppm; and I: 111 ppm. The forward and backward X-ray spectra of a 1 mm thick multi-mineral specimens excited with a Mo anode X-ray beam are shown in Fig. 13. The superposi-

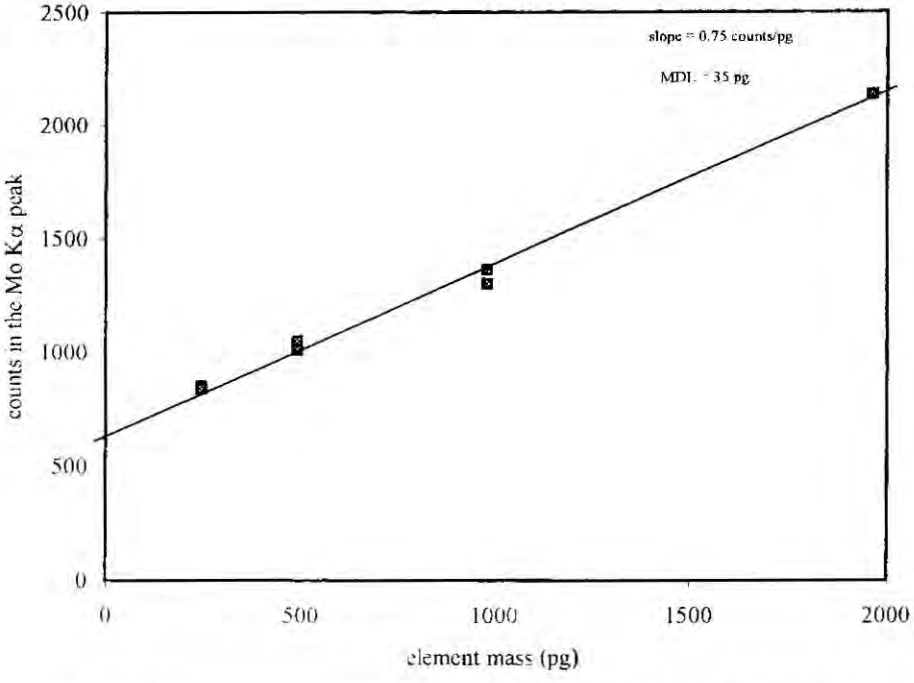

Fig. 11. Calibration curve of FXRF obtained using standard Molybdenum solutions.

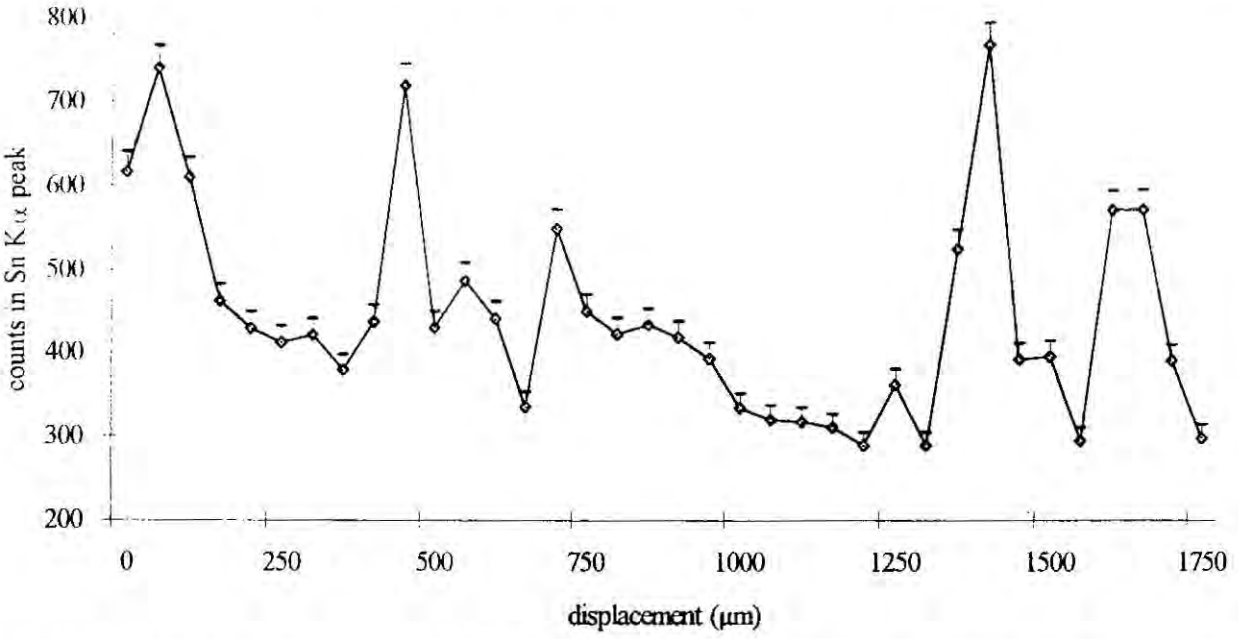

Fig. 12. Scan of an epoxy disk embedded with 20–100 μm grains of tin. The incident beam was collimated to 5 μm and the geometry as shown in Fig. 2 was utilised.

tion of the two spectra is in good agreement with the results of Fig. 8.

An interesting aspect of the FXRF is the enhancement of the fluorescence of characteristic X rays of intermediate Z elements with respect to lower Z elements. This is demonstrated theoretically in Fig. 14. An example of this effect is shown in Fig. 15 which includes the FXRF and BXRF spectra of a 1 mm thick sample of marine sediment. This figure demonstrates the enhancement of the Strontium and Zirconium fluorescence signal in a lighter matrix.

5. Conclusions

The advantages of the FXRF with respect to the usual normal XRF are mainly three:

(a) *Geometrical:* FXRF can result in a very compact geometry since the sample–detector (r_D) and sample–source (r_S) distances can be reduced. Additionally, the geometrical efficiency can be improved.

(b) *Volumetric:* a small volume is analysed, with the additional advantage of the interaction volume being nearly cylindrical in shape. In the FXRF, this cylinder can be normal to the surface of the sample.

(c) *Analytical:* the fluorescence of intermediate atomic number elements can be enhanced when they are being analysed in the presence of low atomic number elements.

The following conclusions can be deduced for the FXRF analysis.

(1) *Thin samples:* For thin samples the advantage of the FXRF-method arises from the geometrical efficiency that, for an equal irradiated volume, it can be maximised (Eq. (11)). The geometrical efficiency is very important when microanalysis, and/or the elemental distributions within a sample are required; FXRF is inherently more efficient and the uncertainties in the volumes sampled are minimized. A disadvantage may be the fact that the total count rate in the spectrum is higher.

(2) *Intermediate samples:* For intermediate thickness samples the advantages of FXRF arise

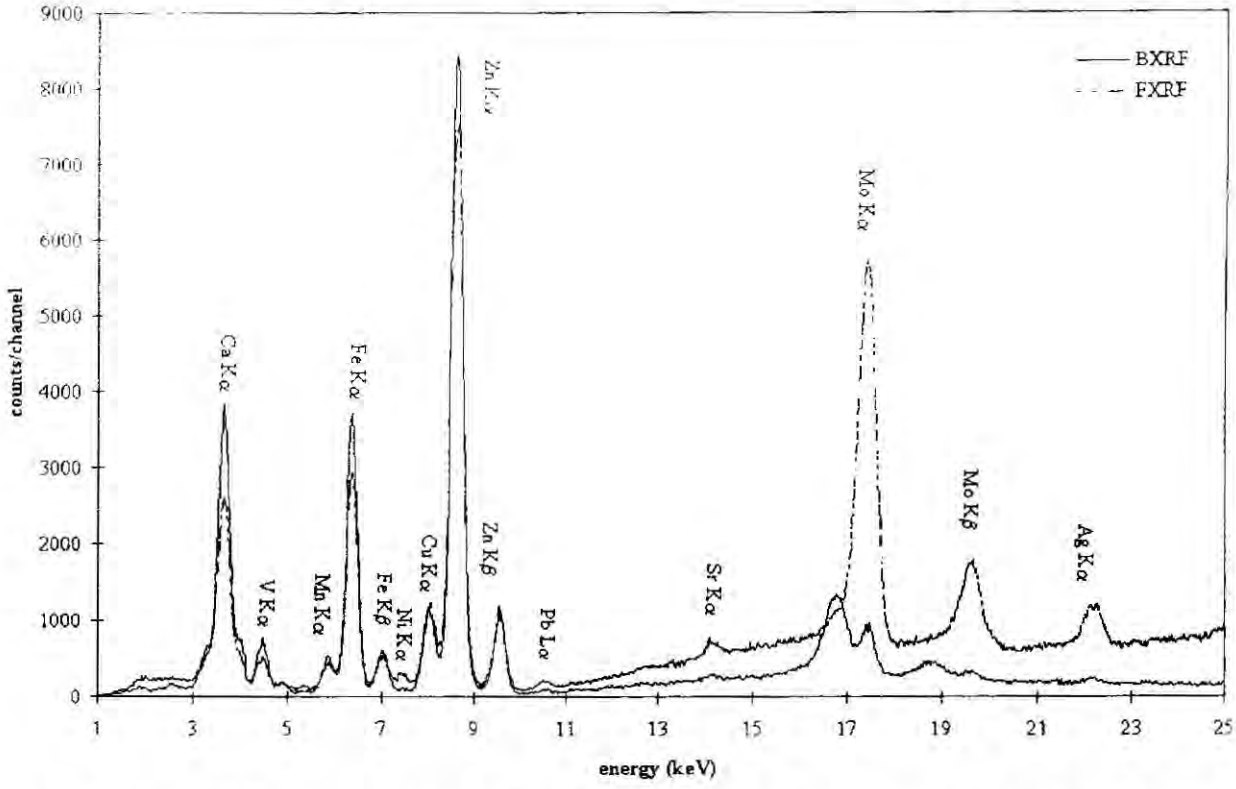

Fig. 13. FXRF and BXRF spectra of a thin sample of a multi-mineral pastille. The two spectra have been obtained with Mo anode X-ray beam. In the BXRF spectrum the Compton is shifted toward a lower energy.

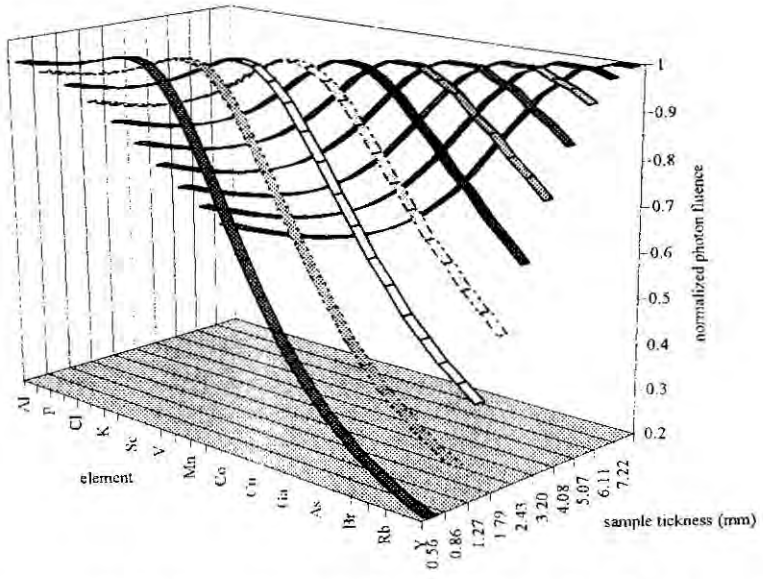

Fig. 14. Relative fluorescence flux for K_γ-lines of elements in the interval between Ca and Y at some sample thickness. The enhancement of fluorescent flux of intermediate elements is due to the filter action of the sample itself.

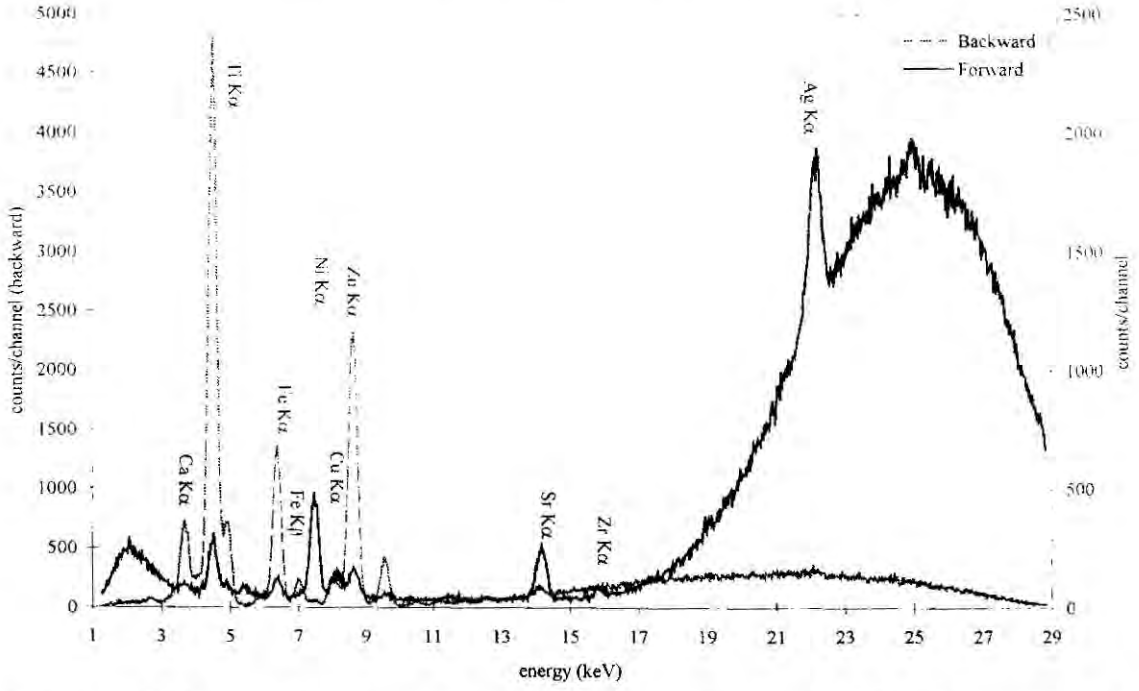

Fig. 15. BXRF and FXRF spectra of a thick marine sediment sample W anode X-ray beam (HV 35 KV). The "amplification" of Rb, Sr, Zr and Ag peaks with respect to Fe-peak is evident.

from geometrical, volumetric and elemental considerations. For FXRF the geometrical efficiency is larger, and the volume definition is better. Additionally there is the possibility of enhancing the fluorescence of higher Z elements with respect to lower Z elements. The simultaneous detection of the FXRF and BXRF intensities can be used to correct for the self-absorption effect.

(3) *Thick samples:* For thick samples FXRF shows no benefit.

Acknowledgements

This work was performed under the auspices of the US Department of Energy in the case of A.L. Hanson. The submitted manuscript has been authored under Contract No. DE-AC02-98CH10886 with the US Department of Energy. Accordingly, the US Government retains a non-exclusive, royalty-free license to publish or reproduce the published form of the contribution, or allow others to do so, for US Government purposes.

References

[1] R. Klockenkämper, B. Raith, S. Divoux, B. Gonsior, S. Brüggerhoff, E. Jackwerth, Fresenius Z. Anal. Chem. 326 (1987) 108.
[2] B. Williams, Compton Scattering, McGraw-Hill, New York, 1977.
[3] M. Cooper, Adv. Phys. 20 (1971) 453.
[4] A. Markowicz, R. Van Grieken, Quantification in XRF analysis of intermediate-thickness samples, in: R. Van Grieken, A. Markowicz (Eds.), Handbook on X-Ray Spectrometry: Methods and Techniques, Marcel Dekker, New York, 1992, pp. 339–357.
[5] D.E. Eastman, Y. Farge (Eds.), Handbook on Synchrotron Radiation, North-Holland, Amsterdam, 1983
[6] R. Cesareo, Photon induced X-ray emission, in: R. Cesareo (Ed.), Nuclear Analytical Techniques in Medicine, Elsevier, Amsterdam, New York, Tokio 1988.
[7] R.Cesareo, A. De Almeida, D.V. Rao, Quasi monochromatic X-rays produced with tubes through transmission and diffusion filters; Centro Interdipartimentale di Ricerca sull'Analisi dei Modelli e dell'Informazione nei Sistemi Biomedici, Università di Roma "La Sapienza"; Int. Rep. 02.93, 1993.
[8] A. Mendoza, J.J. Meitin, R. Cesareo, F. de la Fuente, Absolute emission-transmission method of energy dispersive X ray fluorescence for micro-algae analysis: Centro

Interdipartimentale di Ricerca sull'Analisi dei Modelli e dell'Informazione nei Sistemi Biomedici, Università di Roma "La Sapienza"; Int. Rep. 01.96, 1996.
[9] AMPTEK Inc., Bedford, MA 01730-2204, USA.
[10] J.R. Rhodes, Design and application of X ray emission analysers using radioisotope X ray and γ-ray sources; Special Technical Publication 485, American Society for Testing and Materials, Philadelphia, Pa 19103, 1971.
[11] R. Cesareo, S. Mascarenhas, Nucl. Instr. and Meth. A 277 (1989) 669.